MARCUS VINICIUS OLIVEIRA PACHECO

NAVEGAÇÃO POR GPS AUXILIADA POR ODOMETRIA PARA ROBÓTICA MÓVEL:

COMPARAÇÃO ENTRE INTEGRAÇÕES FRACAMENTE E FORTEMENTE ACOPLADAS SOB CONDIÇÕES RESTRITAS DE VISIBILIDADE DE SATÉLITE

LAVRAS – MG

2023

MARCUS VINICIUS OLIVEIRA PACHECO

NAVEGAÇÃO POR GPS AUXILIADA POR ODOMETRIA PARA ROBÓTICA MÓVEL:

COMPARAÇÃO ENTRE INTEGRAÇÕES FRACAMENTE E FORTEMENTE ACOPLADAS SOB CONDIÇÕES RESTRITAS DE VISIBILIDADE DE SATÉLITE

Trabalho de Conclusão de Curso apresentado à Universidade Federal de Lavras, como parte das exigências do Curso de Engenharia de Controle e Automação, para a obtenção do título de Bacharel.

Prof. DSc. Felipe Oliveira e Silva

Orientador

LAVRAS – MG

2023

Ficha catalográfica elaborada pelo Sistema de Geração de Ficha Catalográfica da Biblioteca Universitária da UFLA, com dados informados pelo(a) próprio(a) autor(a).

Pacheco, Marcus Vinicius Oliveira

Navegação por GPS auxiliada por odometria para Robótica Móvel : Comparação entre integrações fracamente e fortemente acopladas sob condições restritas de visibilidade de satélite / Marcus Vinicius Oliveira Pacheco. – Lavras : UFLA, 2023.

18 p. :

TCC (graduação)–Universidade Federal de Lavras, 2023.

Orientador: Prof. DSc. Felipe Oliveira e Silva.

Bibliografia.

1. Navegação. 2. GPS. 3. Odometria. I. Silva, Felipe Oliveira e. II. Título.

MARCUS VINICIUS OLIVEIRA PACHECO

NAVEGAÇÃO POR GPS AUXILIADA POR ODOMETRIA PARA ROBÓTICA MÓVEL: COMPARAÇÃO ENTRE INTEGRAÇÕES FRACAMENTE E FORTEMENTE ACOPLADAS SOB CONDIÇÕES RESTRITAS DE VISIBILIDADE DE SATÉLITE

GPS-AIDED ODOMETRY NAVIGATION FOR MOBILE ROBOTICS: COMPARISON BETWEEN LOOSELY AND TIGHTLY COUPLED INTEGRATIONS UNDER RESTRICTED SATELLITE VISIBILITY CONDITIONS

Trabalho de Conclusão de Curso apresentado à Universidade Federal de Lavras, como parte das exigências do Curso de Engenharia de Controle e Automação, para a obtenção do título de Bacharel.

APROVADA em 01 de Agosto de 2023.

Prof. DSc. Arthur de Miranda Neto UFLA
MSc. Gustavo de Souza Carvalho BYD

Prof. DSc. Felipe Oliveira e Silva
Orientador

LAVRAS – MG
2023

AGRADECIMENTOS

À minha família, minhas irmãs Laura e Sara, e principalmente minha mãe Érica e meu pai Vinícius, que me apoiram durante todo o meu curso.

Ao meu professor Felipe, que me orientou durante o trabalho, me apoiou e me guiou dentro da área de navegação em diversos trabalhos acadêmicos científicos nesses anos.

À Equipe TROIA de Robótica, que ajudou no protótipo de IAR e foi a minha casa na Universidade, me abrindo o mundo na área de robótica, eletrônica e mecânica.

Quando penso que cheguei ao meu limite, descubro que tenho forças para ir além.
(Ayrton Senna)

RESUMO

Atualmente, a navegação de veículos inteligentes é predominantemente dependente de Sistemas Globais de Navegação por Satélites (GNSS) baseados em posicionamento Cinemático em Tempo-Real (RTK), particularmente o Sistema de Posicionamento Global (GPS). Uma das aplicações da robótica móvel é a Agricultura de precisão (PA), que por exigir um posicionamento preciso, tal tecnologia se torna financeiramente inviável para pequenos e médios agricultores, que são a maioria no Brasil. Por outro lado, a odometria pode servir como uma tecnologia de navegação mais econômica (ou ainda complementar) ao GPS. Apesar de seu conhecido acúmulo de erros ao longo da distância percorrida, a odometria fornece soluções de posicionamento satisfatórias a curto prazo. Assim, o objetivo deste estudo é avaliar o desempenho de uma solução de navegação por odometria auxiliada por GPS de baixo custo, i.e., de Simples Frequência (SF), visando aumentar a precisão de posicionamento de Robôs Inteligentes. A principal contribuição desta pesquisa envolve a extensão de pesquisas anteriores sobre duas técnicas de integração comumente usadas em aplicações de fusão de sensores, ou seja, as topologias Fracamente Acopladas (LC) e Fortemente Acopladas (TC), no cenário específico de sinais GNSS eventualmente bloqueados, ou seja, quando a Visibilidade do Satélite (SV) é gradualmente prejudicada. São fornecidos resultados experimentais que destacam a superioridade da solução TC, mesmo quando apenas 2 satélites estão à vista.

Palavras-chave: Navegação, GPS, Visibilidade, Odometria, Robótica.

ABSTRACT

In modern times, the navigation of intelligent vehicles is predominantly reliant on Real Time Kinematics (RTK)-based Global Navigation Satellite Systems (GNSS), particularly the Global Positioning System (GPS). One of the applications of mobile robotics is Precision Agriculture (PA), which requires precise positioning, such technology becomes financially unfeasible for small and medium-sized farmers, who are the majority of farmers in Brazil. On the other hand, odometry can serve as a cost-effective alternative (or complementary navigation technology) to GPS. Despite its well-known error accumulation over the traveled distance, odometry provides satisfactory short-term positioning solutions. Thus, the objective of this study is to evaluate the performance of a low-cost Single-Frequency (SF) GPS-aided odometry navigation solution, aiming at enhancing positioning accuracy for Intelligent Robots. The primary contribution of this research involves extending previous research about two integration techniques commonly used in sensor fusion applications, namely the Loosely Coupled (LC) and Tightly Coupled (TC) topologies, in the specific scenario of GNSS signals becoming eventually blocked, i.e., when Satellite Visibility (SV) is gradually impaired. Experimental results are provided, which highlight the superiority of the TC solution, even when only 2 satellites are in view.

Keywords: Navigation, GPS, Visibility, Odometry, Robotics.

LISTA DE FIGURAS

LISTA DE TABELAS

SUMÁRIO

1 INTRODUÇÃO

As soluções de navegação de precisão representam um desafio na Robótica Móvel, em especial para os pequenos e médios agricultores brasileiros interessados em implementar técnicas de Agricultura de Precisão (AP), como a utilização de Robôs Agrícolas Inteligentes (IARs) (MIRANDA; VERÍSSIMO; CEOLIN, 2017). Até 2022, 77% dos agricultores brasileiros eram considerados como tal, ou seja, agricultores familiares. Enquanto a convencional e amplamente utilizada técnica de posicionamento Cinemático em Tempo-Real (RTK) baseada em Sistemas de Navegação Global por Satélites (GNSS) mutil-frequência e multi-constelação ainda pode ser proibitivo em termos de custo para o último (MAHATO et al., 2019), a aplicação de técnicas de baixo custo como o Posicionamento de Ponto Preciso em Tempo Real de Frequência Única (SF-RT-PPP) ainda é limitada devido à falta de cobertura total de internet no campo, como forma de se obter correções de posicionamento (RAHMAN et al., 2022).

Além disso, depender apenas do GNSS como solução de navegação para esses usuários gera desvantagens adicionais: (a) a incapacidade dos receptores GNSS de fornecer informações precisas de atitude (orientação), particularmente para robôs em baixa velocidade, as quais são requsitos em PA (MIRANDA; VERÍSSIMO; CEOLIN, 2017); (b) a suscetibilidade dos sinais GNSS a interrupções, isolamentos, bloqueios, interferências e falsificações (FARRELL, 2008); (c) a falta de um Sistema Brasileiro de Aumento Baseado em Satélite (SBAS) gratuito semelhante ao Sistema de Aumento de Área Ampla (WAAS) disponível para usuários do Sistema de Posicionamento Global (GPS) na América do Norte (PEREIRA, 2022); e (d) a baixa densidade de Estações de Referência de Operação Contínua (CORS) gratuitas, especialmente nas regiões centro e norte do Brasil, para usuários interessados em implementar estratégias de posicionamento Diferencial (DGNSS) e/ou Relativo (RGNSS).

Como solução alternativa de posicionamento para Robôs Inteligentes, tem-se a implantação de técnicas *Dead-Reckoning* (DR), como navegação inercial e por odometria de rodas (MARTINS et al., 2011). A odometria, em particular, é uma solução reconhecidamente de baixo custo, capaz de proporcionar um bom desempenho de navegação, desde que sejam satisfeitas algumas condições, nomeadamente: (a) a superfície de deslocamento do veículo é plana; (b) um bom procedimento de inicialização pode ser conduzido; (c) implementa-se a estimativa/-compensação em tempo real das variações dos raios das rodas (ONYEKPE et al., 2020); e (d) os eventos de escorregamento e derrapagem são minimizados por meio, por exemplo, do uso de

algoritmos de detecção de *outliers* e da montagem dos *encoders* nas rodas não tracionadas do robô (GROVES, 2013).

Este estudo baseia-se em pesquisas anteriores disponíveis na literatura (PEREIRA; SILVA, 2023), que exploraram o potencial de obtenção de posicionamento preciso para IARs por meio da integração de receptores GPS de frequência única (SF) e sensores odométricos de baixo custo por meio de um Filtro de Kalman Estendido (EKF). Enquanto em (PEREIRA; SILVA, 2023), os autores se concentraram em avaliar o desempenho das topologias de integração Fracamente Acoplada (LC) e Fortemente Acoplada (TC) quando a odometria estava sujeita a circunstâncias adversas, aqui o interesse é comparar os esquemas de integração supracitados, quando o GPS torna-se gradativamente indisponível, ou seja, quando a Visibilidade do Satélite (SV) começa a ficar comprometida (simulando, por exemplo, um cenário de um IAR sob uma densa vegetação ou cobertura vegetal).

A principal contribuição deste estudo é a demonstração de que a navegação por odometria auxiliada por GPS baseada em TC apresenta robustez significativamente maior em comparação com a abordagem LC, considerando uma situação em que os sinais GNSS são mais vulneráveis a bloqueios, especialmente quando o número de satélites visíveis cai abaixo de três.

GPS-Aided Odometry Navigation for IARs: Comparison Between Loosely and Tightly Coupled Integrations Under Restricted Satellite Visibility Conditions

1st Marcus Vinicius O. Pacheco
Department of Automatics
Federal University of Lavras
Lavras, Brazil
marcus.pacheco@estudante.ufla.br

2nd Felipe O. Silva
Department of Automatics
Federal University of Lavras
Lavras, Brazil
felipe.oliveira@ufla.br

***Abstract*—In modern times, the navigation of agricultural vehicles is predominantly reliant on Real Time Kinematics (RTK)-based Global Navigation Satellite Systems (GNSS), particularly the Global Positioning System (GPS). However, when precise positioning is required, as is often the case in Precision Agriculture (PA), this technology becomes financially unfeasible for small and medium-sized farmers, who are the majority of farmers in Brazil. On the other hand, odometry can serve as a cost-effective alternative (or complementary navigation technology) to GPS. Despite its well-known error accumulation over the traveled distance, odometry provides satisfactory short-term positioning solutions. Thus, the objective of this study is to evaluate the performance of a low-cost Single-Frequency (SF) GPS-aided odometry navigation solution, aiming at enhancing positioning accuracy for Intelligent Agricultural Robots (IARs). The primary contribution of this research involves extending previous research about two integration techniques commonly used in sensor fusion applications, namely the Loosely Coupled (LC) and Tightly Coupled (TC) topologies, in the specific scenario of GNSS signals becoming eventually blocked, i.e., when Satellite Visibility (SV) is gradually impaired. Experimental results are provided, which highlight the superiority of the TC solution, even when only 2 satellites are in view.**

***Index Terms*—navigation, GPS, visibility, odometry, agriculture**

I. Introduction

Precision navigation solutions pose a challenge for small and medium-sized Brazilian farmers who are interested in implementing Precision Agriculture (PA) techniques, such as utilizing Intelligent Agricultural Robots (IARs) [1]. By 2022, 77% of the Brazilian farmers were considered as such, i.e., family farmers. While the conventional and widely used Real Time Kinematics (RTK) based on multi-frequency, multi-constellation Global Navigation Satellite System (GNSS) equipment may still be cost-prohibitive for the latter [2], the application of low-cost techniques like Single-Frequency Real-Time Precise Point Positioning (SF-RT-PPP) is still limited due to the lack of full internet coverage in the field, as a mean of obtaining positioning corrections [3].

Furthermore, relying solely on GNSS as a navigation solution for these users faces additional drawbacks: (a) the inability of GNSS receivers to provide accurate attitude (orientation) information, particularly for low-speed IARs, as required in PA [1]; (b) the susceptibility of GNSS signals to outages, outliers, blockages, jamming and spoofing [4]; (c) the lack of a free-of-cost Brazilian Satellite-Based Augmentation System (SBAS) similar to the Wide Area Augmentation System (WAAS) available for Global Positioning System (GPS) users in North America [5]; and (d) the low density of free-of-cost Continuously Operating Reference Stations (CORS), specially in the central and north areas of Brazil, for users interested in deploying Differential (DGNSS) and/or Relative (RGNSS) positioning strategies.

As an alternative positioning solution for IARs, one has the deployment of Dead-Reckoning (DR) techniques, such as inertial and wheel odometry navigation [6]. Odometry, in particular, is a recognizably low-cost solution, which is able to deliver good navigation performance, provided that a few conditions are fulfilled, namely: (a) the displacement surface of the vehicle is flat; (b) a good initialization procedure has been conducted; (c) real-time estimation/compensation of the wheel radius variations is in line [7]; and (d) slipping and skidding events are minimized via, for instance, the use of outlier detection algorithms and the encoder sensors mounting on the IAR's non-driven wheels [8]. Unfortunately, for PA applications, most the aforementioned requirements are not easily met.

This study builds upon previous research available in the literature [9], which explored the potential of achieving accurate positioning for IARs through the integration of Single-Frequency (SF) GPS and low-cost odometry sensors via an Extended Kalman Filter (EKF). While in [9], the authors focused on assessing the performance of the Loosely Coupled (LC) and Tightly Coupled (TC) integration topologies when odometry was subject to adverse circumstance, here we are interested in comparing the aforementioned integration schemes, when

GNSS becomes gradually unavailable, i.e., when Satellite Visibility (SV) begins to be compromised (simulating, hence, a scenario of an IAR being under a dense vegetation or tree canopy, for instance).

The main contribution of this study is the demonstration that TC-based GPS-aided odometry navigation exhibits significantly greater robustness compared to the LC approach, considering a situation when GNSS signals are more vulnerable to blockages, specially when the number of visible satellites drops below three.

The remainder of this paper is structured as follows: Section II elaborates on the LC and TC topologies implemented in the proposed EKF-based GPS-aided odometry navigation solution for IARs; in Section III, results from an experimental test are presented, considering a restricted number of visible satellites; finally, Section IV concludes the article and offers additional insights.

II. Odometry/GPS Integration

The integration technique proposed in this study is based on the so-called "error state implementation" [4], [8], wherein an EKF is used to estimate and correct errors in the navigation variables (provided, in the case, by the odometry), as well as sufficiently observable systematic errors in GPS measurements. The latter can be further classified as TC or LC depending on the type of GPS measurement used in the EKF update step. Next, we present the main structure of the integration EKF, while more detailed information on the practical implementation of individual odometry, GPS, and the integrated navigation solution can be found in [4], [5], [8].

A. EKF Prediction Step

To perform the EKF prediction step in both LC and TC GPS-aided odometry navigation solutions, it is necessary to establish appropriate dynamic and error models for the state variables to be estimated. In the LC integration filter, the state vector $\mathbf{x}_{LC}$ consists solely of the errors (designated as δ) in the odometry navigation solution:

$$\mathbf{x}_{LC} = \begin{bmatrix} \delta\psi & \delta r^n_{eb,N} & \delta r^n_{eb,E} & \delta R_{rL} & \delta R_{rR} \end{bmatrix}^T \tag{1}$$

In this context, $\delta\psi$ represents the error in yaw measurement from odometry, $\delta r^n_{eb,N}$ denotes the error in north position measurement from odometry, $\delta r^n_{eb,E}$ represents the error in east position measurement from odometry, and δR_{rL} and δR_{rR} are the biases associated with the radius of the IAR's left (subscript L) and right (subscript R) wheels, respectively[1].

In the case of TC integration, the state vector $\mathbf{x}_{TC}$ is expanded to include the GPS receiver clock error $\delta\rho^a_c$ and drift $\delta\dot{\rho}^a_c$:

$$\mathbf{x}_{TC} = \begin{bmatrix} \mathbf{x}^T_{LC} & \delta\rho^a_c & \delta\dot{\rho}^a_c \end{bmatrix}^T \tag{2}$$

The process model for the integration EKF is established based on the dynamic equations that govern the temporal evolution of the odometry error states. Specifically, in the case of TC integration, the process model can be described as follows:

$$\dot{\mathbf{x}}_{TC} = \begin{bmatrix} 0 & 0 & 0 & F_{14} & F_{15} & 0 & 0 \\ F_{21} & 0 & 0 & F_{24} & F_{25} & 0 & 0 \\ F_{31} & 0 & 0 & F_{34} & F_{35} & 0 & 0 \\ 0 & 0 & 0 & -\frac{1}{\tau_{R_r}} & 0 & 0 & 0 \\ 0 & 0 & 0 & 0 & -\frac{1}{\tau_{R_r}} & 0 & 0 \\ 0 & 0 & 0 & 0 & 0 & 0 & 1 \\ 0 & 0 & 0 & 0 & 0 & 0 & 0 \end{bmatrix} \mathbf{x}_{TC} + \begin{bmatrix} \frac{1}{T_r} & -\frac{1}{T_r} & 0 & 0 & 0 & 0 \\ G_{21} & G_{22} & 0 & 0 & 0 & 0 \\ G_{31} & G_{32} & 0 & 0 & 0 & 0 \\ 0 & 0 & 1 & 0 & 0 & 0 \\ 0 & 0 & 0 & 1 & 0 & 0 \\ 0 & 0 & 0 & 0 & 1 & 0 \\ 0 & 0 & 0 & 0 & 0 & 1 \end{bmatrix} \begin{bmatrix} R_{rL}\delta\omega_{rL} \\ R_{rR}\delta\omega_{rR} \\ \eta_{R_{rL}} \\ \eta_{R_{rR}} \\ \eta_{\rho^a_{c\phi}} \\ \eta_{\rho^a_{cf}} \end{bmatrix} \tag{3}$$

with,

$$F_{14} = \frac{v_{erL}}{R_{rL}T_r} \tag{4}$$

$$F_{15} = -\frac{v_{erR}}{R_{rR}T_r} \tag{5}$$

$$F_{21} = -\sin\psi v_{er} + \left(-\sin\psi l^b_{br,y} + \cos\psi l^b_{br,x}\right)\dot{\psi} \tag{6}$$

$$F_{24} = \frac{\cos\psi v_{erL}}{2R_{rL}} + \left(\frac{\cos\psi l^b_{br,y} + \sin\psi l^b_{br,x}}{T_r R_{rL}}\right) v_{erL} \tag{7}$$

$$F_{25} = \frac{\cos\psi v_{erR}}{2R_{rR}} - \left(\frac{\cos\psi l^b_{br,y} + \sin\psi l^b_{br,x}}{T_r R_{rR}}\right) v_{erR} \tag{8}$$

$$F_{31} = \cos\psi v_{er} + \left(\cos\psi l^b_{br,y} + \sin\psi l^b_{br,x}\right)\dot{\psi} \tag{9}$$

$$F_{34} = \frac{\sin\psi v_{erL}}{2R_{rL}} + \left(\frac{\sin\psi l^b_{br,y} - \cos\psi l^b_{br,x}}{T_r R_{rL}}\right) v_{erL} \tag{10}$$

$$F_{35} = \frac{\sin\psi v_{erR}}{2R_{rR}} - \left(\frac{\sin\psi l^b_{br,y} - \cos\psi l^b_{br,x}}{T_r R_{rR}}\right) v_{erR} \tag{11}$$

$$G_{21} = \frac{\cos\psi}{2} + \left(\frac{\cos\psi l^b_{br,y} + \sin\psi l^b_{br,x}}{T_r}\right) \tag{12}$$

$$G_{22} = \frac{\cos\psi}{2} - \left(\frac{\cos\psi l^b_{br,y} + \sin\psi l^b_{br,x}}{T_r}\right) \tag{13}$$

$$G_{31} = \frac{\sin\psi}{2} + \left(\frac{\sin\psi l^b_{br,y} - \cos\psi l^b_{br,x}}{T_r}\right) \tag{14}$$

$$G_{32} = \frac{\sin\psi}{2} - \left(\frac{\sin\psi l^b_{br,y} - \cos\psi l^b_{br,x}}{T_r}\right) \tag{15}$$

In (3)-(15), the correlation time for the radius error of the rear wheels is denoted as τ_{R_r}; the length of the rear axle is represented by T_r; the speed of the center of the rear axle is given by v_{er}; the left and right rear wheel speeds are denoted as v_{erL} and v_{erR}, respectively; the lever arm between the body

[1]Throughout this work, we assume a rear-wheel odometry navigation.

and rear wheel coordinate frames is defined by $l^b_{br,x}$ and $l^b_{br,y}$, which correspond to its x and y components, respectively[2]; $\delta\omega_{rL}$ and $\delta\omega_{rR}$ represent the Gaussian white noises associated with the numerical quantization process of the odometer pulses on the left and right rear wheels, respectively; the Gaussian white driven-noises of the correlated processes adopted to model the left and right wheel radius errors are denoted as $\eta_{R_{rL}}$ and $\eta_{R_{rR}}$, respectively; and lastly, $\eta_{\rho^a_{c\phi}}$ and $\eta_{\rho^a_{cf}}$ are the Gaussian white noises used to model the uncertainties in the phase and frequency of the GPS receiver clock.

To account for the impact of all these noises in the EKF estimation process, the corresponding process noise density matrix needs to be properly adjusted for optimal accommodation:

$$S_{TC} = \begin{bmatrix} PSD(R_{rL}\delta\omega_L) & \cdots & 0 \\ \vdots & \ddots & \vdots \\ 0 & \cdots & PSD(\eta_{\rho^a_{cf}}) \end{bmatrix} \tag{16}$$

where PSD denotes Power Spectral Density.

B. EKF Update Step: LC Integration

In the LC integration of the GPS-aided odometry navigation solution, the EKF measurement innovations $\boldsymbol{z}_{LC}$ are determined as the difference between the Cartesian Earth-Centered-Earth-Fixed (ECEF)[3] position measured by the GPS, denoted as $\tilde{\mathbf{r}}^e_{eb,G}$, and the corresponding estimate from odometry, represented as $\hat{\mathbf{r}}^e_{eb}$. In terms of measurement model, this relationship can be expressed as follows:

$$\mathbf{z}_{LC} = \begin{bmatrix} 0 & -C^e_{n1,1} & -C^e_{n1,2} & 0 & 0 \\ 0 & -C^e_{n2,1} & -C^e_{n2,2} & 0 & 0 \\ 0 & -C^e_{n3,1} & -C^e_{n3,2} & 0 & 0 \end{bmatrix} \mathbf{x}_{LC} + \begin{bmatrix} 1 & 0 & 0 \\ 0 & 1 & 0 \\ 0 & 0 & 1 \end{bmatrix} \eta_{r^e_{ea,G}} \tag{17}$$

The matrix C^e_n in (17) represents the coordinate transformation matrix from the navigation coordinate frame (subscript n)[4] to the ECEF frame. The term $\eta_{r^e_{ea,G}}$, in turn, represents the GPS position measurements noise vector, which assumed to be white and Gaussian. To accurately leverage the impact of this noise in the integration EKF, the LC measurement noise covariance matrix has to be appropriately adjusted as:

$$R_{LC} = \begin{bmatrix} \sigma^2(\eta_{r^e_{ea,G,x}}) & 0 & 0 \\ 0 & \sigma^2(\eta_{r^e_{ea,G,y}}) & 0 \\ 0 & 0 & \sigma^2(\eta_{r^e_{ea,G,z}}) \end{bmatrix} \tag{18}$$

where σ^2 denotes variance.

[2]The body (subscript b) and rear wheel (subscript r) coordinate frames have their origins at the center of mass of the IAR and at the center of the rear axle, respectively. Additionally, the x, y, and z axes of these frames point frontward, rightward, and downward with respect to the IAR.

[3]The ECEF coordinate frame (subscript e) has its origin at the center of the Earth, with the x-axis pointing to the intersection of the Greenwich Meridian and the Equator, the z-axis pointing in the direction of the Earth's axis of rotation, and the y-axis completing the right-handed orthogonal frame.

[4]The navigation coordinate frame has its origin at the center of mass of the IAR, with its x, y, and z axes pointing to the North, East, and Down (NED) directions, respectively.

C. Update Step: TC Integration

For the TC integration of odometry/GPS, the EKF measurement innovations $\mathbf{z}_{TC}$ are computed as the differences between the pseudo-ranges measured from the GPS receiver antenna to all satellites in view, denoted as $\tilde{\rho}^s_a$, and their corresponding estimates from the odometry navigation solution, represented as $\hat{\rho}^s_a$. Consequently, the measurement model can be expressed as follows:

$$\mathbf{z}_{TC} = \begin{bmatrix} 0 & -u^n_{a1,N} & -u^n_{a1,E} & 0 & 0 & 1 & 0 \\ \vdots & \vdots & \vdots & \vdots & \vdots & \vdots & \\ 0 & -u^n_{as,N} & -u^n_{as,E} & 0 & 0 & 1 & 0 \end{bmatrix} \mathbf{x}_{TC} + \begin{bmatrix} 1 & \cdots & 0 \\ \vdots & \ddots & \vdots \\ 0 & \cdots & 1 \end{bmatrix} \begin{bmatrix} \eta^1_\rho \\ \vdots \\ \eta^s_\rho \end{bmatrix} \tag{19}$$

In (19), $u^n_{as,N}$ and $u^n_{as,E}$ represents, respectively, the north and east components of the line-of-sight vector between the satellite s and the receiver antenna a; and η^s_ρ corresponds to the s-th element of the GPS pseudo-range measurement noise vector, which is also assumed to be white and Gaussian.

To accurately model the TC measurement noise covariance matrix, it is recommended in the literature [8], to slightly overestimate the latter, aiming at accounting to, in addition to the receiver tracking noise, any residual satellite ephemeris and clock errors, multipath errors, synchronization errors between the odometry and GPS, line-of-sight-dependent errors and lever arm flexion. Regardless of these effects, it is reasonable to assume that the TC measurement noise covariance matrix is diagonal since there is no correlation between individual measurements:

$$R_{TC} = \begin{bmatrix} \sigma^2(\eta^1_\rho) & \cdots & 0 \\ \vdots & \ddots & \vdots \\ 0 & \cdots & \sigma^2(\eta^s_\rho) \end{bmatrix} \tag{20}$$

III. Experimental Results

To evaluate the effectiveness of the LC and TC GPS-aided odometry navigation solutions for IARs, an experimental test was conducted. The test utilized a custom-built prototype of an IAR, developed by the authors. The latter comprises an extra pair of non-driven rear wheels (wherein the encoder sensors were mounted), positioned parallel to the original pair of driven rear wheels (Figure 1). The following apparatuses were onboard the IAR during the test:

- A u-blox® C102-F9R integrated navigation module, which provided raw SF GPS data[5] for off-line processing of the integration algorithms under investigation, as well as the Ground-Truth (GT) navigation solution for comparison purposes[6];

[5]For the performance assessment of the algorithms, only L1 Coarse Acquisition (C/A) pseudo-range observables from GPS were used.

[6]C102-F9R module embeds a RTK-enabled dual-frequency multi-constellation GNSS-aided Inertial Navigation System (INS), which is able to deliver position solutions accurate at the centimeter level [10].

Fig. 1. IAR utilized in the test.

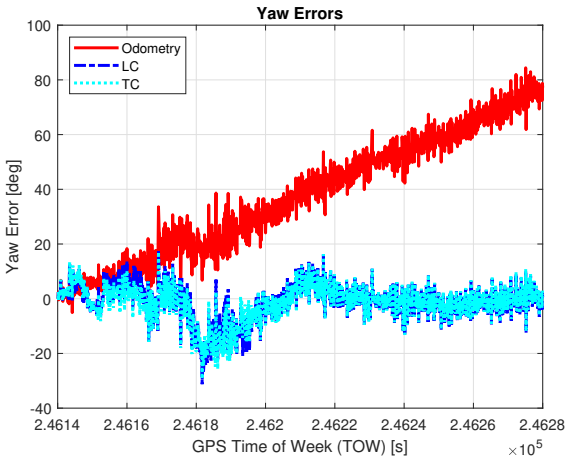

Fig. 2. Yaw error for the unrestricted SV scenario

- Two LPD 3806 rotary encoders with resolution of 400 pulses per revolution;
- An Arduino® MEGA 2560 board for acquiring the pulses from the encoders and synchronizing the latter with income messages from the C102 module;
- A laptop computer for collecting the C102 module data via u-center software and saving the Arduino® board data in text format;
- A pair of electric motors for propulsion;
- A lithium-polymer battery to power the motors;
- An electronic speed controller board to control the IAR according to radio commands.

The experimental test consisted on driving the IAR along a dirt road, which was surrounded by a few trees and small buildings. The test took place on a day with clear sky, i.e., free from significant cloud cover. The IAR traveled a distance of about 150 meters at an average speed of 4 km/h. All necessary data for evaluating the performance of the integrated odometry/GPS navigation solutions were gathered and saved for offline processing using MATLAB® software. After collecting the data, different visibility conditions were simulated by purposely restricting the number of visible GPS satellites through software.

A. LC and TC Performances: Unrestricted SV Scenario

The analysis of the LC and TC topologies was initially conducted without any limitation on the number of visible satellites. Figures 2 to 4 depict the instantaneous errors in the IAR's yaw angle and north/east position estimates, respectively, for the LC and TC SF GPS-aided odometry solutions. Table I, in turn, provides the corresponding mean and Standard Deviation (SD) values. To ensure comparability, results from the odometry-only and SF GPS-only navigation solutions are also included.

As can be seen, the behavior of the odometry-only navigation solution exhibits a pronounced divergence, which aligns with the expected trend of DR methods. This divergence

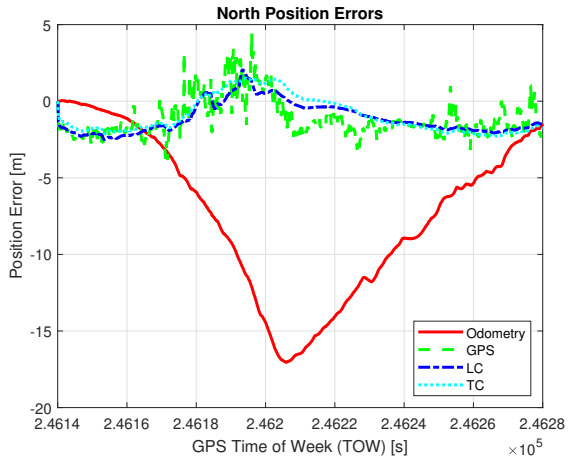

Fig. 3. North position error for the unrestricted SV scenario

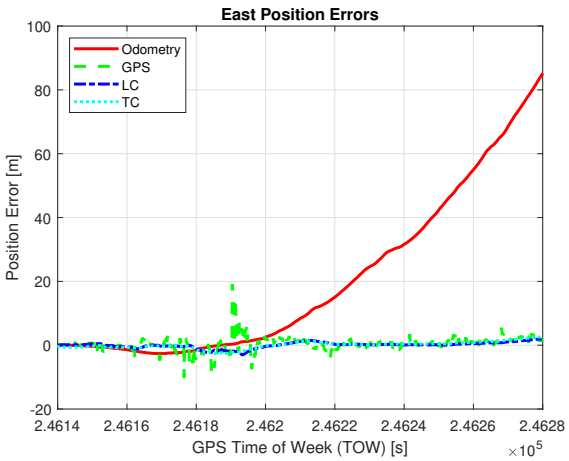

Fig. 4. East position error for the unrestricted SV scenario

TABLE I
MEAN AND SD VALUES FOR THE UNRESTRICTED SV SCENARIO

Error	Odometry	GPS	LC	TC
$\delta\psi$ [deg]	37.52±22.54	—	-1.29±6.65	-1.58±6.50
$\delta r^n_{eb,N}$ [m]	-7.31±5.20	-1.15±1.26	-1.11±1.01	-0.94±1.18
$\delta r^n_{eb,E}$ [m]	20.35±25.53	0.37±2.20	0.01±0.92	0.03±1.10
$\delta r^n_{eb,H}$ [m]	24.64±23.21	2.41±1.44	1.65±0.60	1.75±0.65

is an evidence of the existence of significant biases in the IAR wheel radius, as well as the occurrence of slipping and skidding events during the navigation process. The odometry-only solution performs poorly in terms of position errors, with an accumulated eastward error exceeding 80 meters by the end of the test. In contrast, the GPS-only navigation solution exhibits bounded errors. However, its precision (characterized by the SD values in Table I) is insufficient for most PA applications [1]. Additionally, the GPS-only solution fails to provide orientation information for the IAR unless a trajectory-based approach is adopted [8].

Regarding the navigation performance of both LC and TC GPS-aided odometry solutions, it is evident that they significantly enhance the accuracy and precision of the IAR's yaw angle and position estimates. When compared to the GPS-only navigation solution, LC integration improves the accuracy of north and east positions by 3% and 97%, respectively, while TC integration improves them by 18% and 92%. Similarly, the corresponding precisions are enhanced by 20% and 58% for LC-based integration, and by 6% and 50% for TC integration approach.

The mean and standard deviation values of the horizontal position errors (subscript H) for the investigated navigation solutions are also provided in the last row of Table I. It can be seen that the performances of the LC and TC GPS-aided odometry solutions are quite similar, with a slight tendency of superiority for the LC topology.

B. LC and TC Performances: Restricted SV Scenario

The objective of this work is to evaluate and compare the performance of GPS-aided odometry navigation utilizing LC and TC topologies when GNSS is deemed to be gradually unavailable, i.e., in the advent of loss of SV. In our test, this has been achieved by purposely restricting (via software) the number of GPS satellites that were visible during the test. Table II depicts de GPS Identifier numbers (IDs) of the satellites that were regularly visible, as well as their Elevation Angles (EA) at the beginning of the test. The aforementioned restrictions took place at the instant 40 seconds of the test (GPS Time of Week (TOW) 246180 seconds), and lasted until its end. The SV was restricted following a decreasing order of the GPS IDs, i.e., the first removed satellite was the ID #30, then the ID #20, and so on.

Aiming a more comprehensive assessment of the LC and TC integration topologies under such restricted circumstances, we focused on the evaluation of the Cumulative Distribution Functions (CDF) of the corresponding horizontal position errors, as shown in Figures 5 and 6, wherein UR stands for Unrestricted. As a relevant metric for comparing the CDF results against, we referred to the Society of Automotive Engineering (SAE) standard J2945 [11], which defines a maximum horizontal position error of 1.5 meters, at 68% of probability, aiming at connected autonomous vehicle applications. The main results are summarized in Tables III and IV.

TABLE II
IDS AND ELEVATION ANGLE OF VISIBLE GPS SATELLITES

ID	#5	#7	#13	#14	#17	#19	#20	#30
EA [deg]	20.9	28.8	35.3	60.5	50.8	35.6	20.1	47.0

As can be seen, neither LC nor TC integration approaches were able to meet SAE J2945 positioning requirements, even without restricting the number of visible satellites. The LC approach only achieved a horizontal position accuracy of 1.5

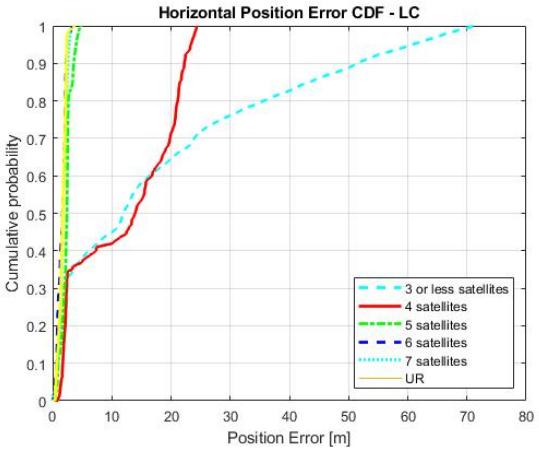

Fig. 5. Horizontal Position Error CDF for LC

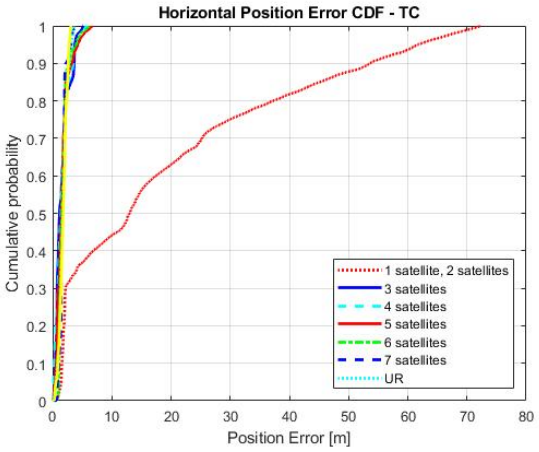

Fig. 6. Horizontal Position Error CDF for TC

TABLE III
PERCENTAGE OF SAMPLES WITH HORIZONTAL POSITION ERROR BELOW 1.5 METER

Integr./SV	1	2	3	4	5	6	7	UR
LC [%]	5.1	5.1	5.1	5.6	16.5	43.4	34.3	38.6
TC [%]	8.2	57.3	55.5	50.8	46.4	37.3	36.4	35.3

TABLE IV
HORIZONTAL POSITION ERROR FOR 68% OF SAMPLES

Integr./SV	1	2	3	4	5	6	7	UR
LC [m]	20.4	20.4	20.4	19.5	2.5	2.0	2.1	2.0
TC [m]	24.4	1.8	1.8	1.8	1.9	1.9	2.1	2.1

meters with a probability of 38%, while the TC approach achieved it at 35% of probability, with all satellites in view available for use.

When it comes to the restricted SV scenario, one sees that an improvement on the latter probability for LC was obtained (43% of samples) when 6 satellites were available. On the other hand, TC was able to deliver horizontal position error below 1.5 meter, at 57% of probability, with only 2 visible satellites. As also shown in Table IV, the TC technique was able to deliver a 1.8 meter error at a 68% of probability, while the LC technique delivered only a 2.0 meter error at the same probability level.

Two additional verifications are worthy of note: (a) for the LC integration topology, one sees that performance was severely impaired when less than 5 satellites were available for use. This is mainly explained by the fact that LC uses GPS position estimates for forming its EKF measurement innovations, which simply cannot be computed when less than 4 satellites are in view. The net results is that, in this case (SV < 4), after the instant 40 seconds of the test, the integrated navigation solution was only maintained by the odometry, which was naturally divergent; and (b) the best results, in terms of horizontal position error, were not obtained, neither for LC nor for TC, when the number of visible satellites was maximum, i.e., unrestricted (as it would be expected). Instead, for LC, the latter was obtained with 6 visible satellites, and for TC with only 2.

Looking at Table II, however, it is possible to associate these outcomes with the EA of the GPS satellites that were visible in each restricted scenario. As it is well known from the literature [8], the smaller the EA, the bigger the corruption of the pseudo-range measurements by CMEs due to ionosphere and especially troposphere propagation. Back to Table II again, one sees that the restricted SV scenario that allowed 7 satellites to be visible, employed the GPS satellite with ID #20, which had low EA. Such satellite was not used in the restricted scenario with SV = 6, which may explain why the horizontal position error results from the former were better than those from the latter. More interestingly to notice is the fact that, for TC under the restricted scenario of SV = 2, only the GPS satellites with IDs #5 and #7 were used, which had relatively low EAs. Despite this, the horizontal positioning performance proved to be good (actually, the best for the entire test), which is an additional evidence of the robustness of the TC topology w.r.t. LC.

IV. CONCLUSIONS

This study examined the performance of SF GPS-aided odometry navigation solutions utilizing LC and TC integration techniques, focusing in situations wherein GNSS signals are prone to blockages, particularly in the context of IARs. Results from an experimental test demonstrated that both strategies effectively improved the positioning accuracy and precision compared to SF GPS-only solution, while also providing reliable orientation information for the IAR. Under the scenario of a restricted number of visible satellites being available for use, TC consistently maintained good results and even exhibited superior positioning performance with only 2 visible satellites. LC, in turn, did not yield satisfactory performance with less than 5 satellites in view.

Despite the positive outcomes reached, the proposed GPS-aided odometry navigation approaches did not meet the positioning accuracy specifications required by SAE J2945 standard. As a proposition for following research, different low-cost aiding sensor approaches, feasible for PA applications, could be explored in the scope of odometry/GPS integration, such as incorporating a cost-effective INS, motion constraints and Zero Updates (ZUPTs).

REFERENCES

[1] A. C. C. de Miranda, A. M. Veríssimo, and A. C. Ceolin, "Agricultura de precisão: Um mapeamento da base da Scielo," *GESTÃO. Org*, vol. 15, no. 6, pp. 129–137, 2017.

[2] S. Mahato, A. Santra, S. Dan, P. Rakshit, P. Benerjee, and A. Bose, "Preliminary results on the performance of cost-effective GNSS receivers for RTK," in *Proceedings of the 2019 URSI Asia-Pacific Radio Science Conference (AP-RASC)*. IEEE, 2019, p. 18760290.

[3] F. Rahman, F. O. Silva, Z. Jiang, and J. A. Farrell, "Low-cost real-time PPP GNSS aided INS for CAV applications," *IEEE Transactions on Intelligent Transportation Systems*, vol. 23, no. 12, pp. 25 018–25 032, 2022.

[4] J. Farrell, *Aided navigation: GPS with high rate sensors*. McGraw-Hill, Inc., 2008.

[5] V. H. L. Pereira, "Navegação odométrica assistida por sistema de posicionamento global para agricultura de precisão," Ph.D. dissertation, Universidade Federal de Lavras, 2022.

[6] R. Martins, S. Bueno, L. Mirisola, E. Paiva, and P. Ferreira, "Localizaçao em robótica terrestre: fusão entre odometria por múltiplos encoders e GPS," *Simpósio Brasileiro de Automação Inteligente (*SBAI*)*, pp. 1043–1048, 2011.

[7] U. Onyekpe, V. Palade, S. Kanarachos, and S.-R. G. Christopoulos, "Learning uncertainties in wheel odometry for vehicular localisation in GNSS deprived environments," in *2020 19th* IEEE *International Conference on Machine Learning and Applications (ICMLA)*. IEEE, 2020, pp. 741–746.

[8] P. D. Groves, *Principles of GNSS, inertial, and multisensor integrated navigation systems*. Artech house, 2013.

[9] V. H. L. Pereira and F. O. Silva, "GPS-aided Odometry Navigation for IAVs: An Assessment of Integration Topologies and Odometry Mounting Configurations," in *Proceedings of the International Instrumentation and Measurement Technology Conference*, vol. 1. IEEE, 2023, pp. 1–6.

[10] ublox, "ZED-F9R module: u-blox F9 high precision dead reckoning module," https://www.u-blox.com/en/product/c102-f9r-application-board, 2022, accessed at 12-09-2022.

[11] SAE, "On-board system requirements for V2V safety communications J2945/1 201603," March 2016.

3 CONCLUSÃO

Este estudo examinou o desempenho de soluções de navegação de odometria auxiliada por receptores GPS de SF utilizando técnicas de integração LC e TC, com foco em situações em que os sinais GNSS são propensos a bloqueios, particularmente no contexto de robôs móveis para agricultura. Os resultados de um teste experimental demonstraram que ambas as estratégias melhoraram efetivamente a exatidão e a precisão do posicionamento em comparação com a solução que utilizou somente GPS, além de fornecer informações de orientação confiáveis para o robô. No cenário de um número restrito de satélites visíveis disponíveis para uso, a topologia TC manteve consistentemente bons resultados, exibindo inclusive, desempenho de posicionamento superior com apenas 2 satélites visíveis. A topologia LC, por sua vez, não apresentou desempenho satisfatório com menos de 5 satélites em vista.

A melhora na precisão com menor número de SV pode ser atribuída à confiabilidade dos dados provenientes dos satélites utilizados. É importante destacar que, quando os satélites possuem um ângulo de elevação mais baixo, tendem a apresentar sinais mais corrompidos pela atmosfera da Terra. Assim, ao retirar satélites com menor ângulo de elevação, foi possível aprimorar a precisão das informações obtidas.

Apesar dos resultados positivos alcançados, as abordagens propostas de navegação por odometria auxiliada por GPS não atenderam às especificações de precisão de posicionamento exigidas pelo padrão SAE J2945. Como proposta para trabalhos futuros, diferentes abordagens de sensores auxiliares de baixo custo, viáveis para aplicações em PA, podem ser exploradas no escopo da integração de odometria/GPS, como a incorporação de um Sistema de Navegação Inercial (INS) de baixo custo, restrições de movimento e Atualizações Estacionárias (ZUPTs).

REFERÊNCIAS

FARRELL, J. **Aided navigation: GPS with high rate sensors**. [S.l.]: McGraw-Hill, Inc., 2008.

GROVES, P. D. **Principles of GNSS, inertial, and multisensor integrated navigation systems**. [S.l.]: Artech house, 2013.

MAHATO, S. et al. Preliminary results on the performance of cost-effective GNSS receivers for RTK. In: IEEE. **Proceedings of the 2019 URSI Asia-Pacific Radio Science Conference (AP-RASC)**. [S.l.], 2019. p. 18760290.

MARTINS, R. et al. Localizaçao em robótica terrestre: fusão entre odometria por múltiplos encoders e GPS. **Simpósio Brasileiro de Automação Inteligente (SBAI)**, p. 1043–1048, 2011.

MIRANDA, A. C. C. de; VERÍSSIMO, A. M.; CEOLIN, A. C. Agricultura de precisão: Um mapeamento da base da Scielo. **GESTÃO. Org**, Universidade Federal de Pernambuco, v. 15, n. 6, p. 129–137, 2017.

ONYEKPE, U. et al. Learning uncertainties in wheel odometry for vehicular localisation in GNSS deprived environments. In: IEEE. **2020 19th IEEE International Conference on Machine Learning and Applications (ICMLA)**. [S.l.], 2020. p. 741–746.

PEREIRA, V. H. L. **Navegação Odométrica Assistida por Sistema de Posicionamento Global para Agricultura de Precisão**. Tese (Doutorado) — Universidade Federal de Lavras, 2022.

PEREIRA, V. H. L.; SILVA, F. O. GPS-aided Odometry Navigation for IAVs: An Assessment of Integration Topologies and Odometry Mounting Configurations. In: IEEE. **Proceedings of the International Instrumentation and Measurement Technology Conference**. [S.l.], 2023. v. 1, p. 1–6.

RAHMAN, F. et al. Low-cost real-time PPP GNSS aided INS for CAV applications. **IEEE Transactions on Intelligent Transportation Systems**, v. 23, n. 12, p. 25018–25032, 2022.

SAE. tech. rep., **On-Board System Requirements for V2V Safety Communications J2945/1 201603**. 2016.

UBLOX. **ZED-F9R module: u-blox F9 high precision dead reckoning module**. 2022. <https://www.u-blox.com/en/product/c102-f9r-application-board>. Accessed at 12-09-2022.